Noncontact Dynamic Oscillations of Acoustically Levitated Particles by Parametric Excitation

A. Dolev,* S. Davis, and I. Bucher
Faculty of Mechanical Engineering, Technion – Israel Institute of Technology, Haifa 3200003, Israel

(Received 26 March 2019; revised manuscript received 4 August 2019; published 16 September 2019)

A method for noncontact particle manipulation is realized here by employing parametric excitation (PE) on levitated particles in acoustic traps. PE enables one to oscillate a particle at one of its natural frequencies in the direction associated with the vibration mode, at a controllable amplitude, while the acoustic traps remain fixed in space. Moreover, the method allows one to select and oscillate a specific particle, while multiple particles are being levitated, by taking advantage of the relatively narrow bandwidth of PE. The underlying principle that allows levitation and PE is based on acoustic radiation forces, which are generated due to nonlinear phenomena in strong ultrasound wave fields. To utilize the method, the levitated particle dynamics within the acoustic trap should be known. Therefore, a lumped parameter model that describes the particle's nonlinear dynamics is derived and its parameters are estimated from measured data. The dynamics of a levitated rigid sphere, when subjected to PE, is studied analytically, numerically, and experimentally. The analytical solution is approximated by the method of multiple scales, and is in a good agreement with the experimental results and numerical simulations. Finally, it is experimentally shown that, if a group of particles is levitated, a specific selected particle can be excited, while the others remain mostly still. It is further shown that the particle's oscillation amplitude can be made so large that it will be ejected from the acoustic trap.

DOI: 10.1103/PhysRevApplied.12.034031

I. INTRODUCTION

Among the various levitation methods developed [1], ultrasonic acoustic levitation is distinguished by its ability to hold and transport any kind of material [2–5]. Acoustic levitation is achieved by producing acoustic radiation forces (ARFs) that counteract gravity. Moreover, ARFs can be applied in a controlled manner for noncontact particle manipulation (NPM) of the levitated object's position and orientation [3,6–8]. Recently, holographic acoustic tweezers were introduced by Marzo and Drinkwater [9], which enabled simultaneous control and manipulation of multiple particles. NPM techniques are used for various applications, such as chemical analysis [10,11], containerless processing [12], measurement [13], and transport [14]. ARFs are generated in strong acoustic fields via nonlinear phenomena [6,15,16]. Within ultrasound wave fields, acoustic "traps" [17] are created in locations of ARF convergence. These traps can be used to hold particles in space, and their spatial geometry depends mostly on the ultrasound frequency and acoustic levitator's geometry [18]. Ultrasonic NPM is not commonplace and has previously been realized only by translation and rotation of the acoustic traps [6], where the dynamics of the particle within the acoustic field is largely ignored [6,8,19], although Fushimi *et al.* [20] considered it. In addition, at least two transducers are needed to manipulate acoustic traps, although recently 2D NPM using a single transducer was reported [21]. Furthermore, the relationship between the levitator's geometry, ultrasonic transducer parameters, and the generated ultrasound wave field should be known [8]. These requirements may lead to sophisticated, although complex to realize, methods [6,9].

The particle dynamics in a 3D acoustic trap is governed by nonlinear conservative and dissipative forces, which are controlled by four physical effects: acoustic radiation forces, acoustic streaming, inertia, and viscous drag [22]. Considering small amplitude oscillations, the particle position can be represented with a coordinate system aligned with the stiffness matrix principal axes. This implies that the particle is held in space by three orthogonal linear springlike forces. Therefore, by exciting the particle at a frequency close to one of the three resonance frequencies, it will oscillate in the direction associated with the appropriate vibration mode [see Figs. 1(b) and 1(c), Sec. IV C, and Video 5 [23]]. By increasing the excitation level, and thus, the oscillation amplitude, the particle can be ejected from the acoustic trap in a desired direction [see Fig. 1(f), Sec. IV B and Video 3 [23]]. In practice, when large oscillation amplitudes occur, nonlinear stiffness and damping terms must be considered [20,24–26].

*amitdtechnion@gmail.com

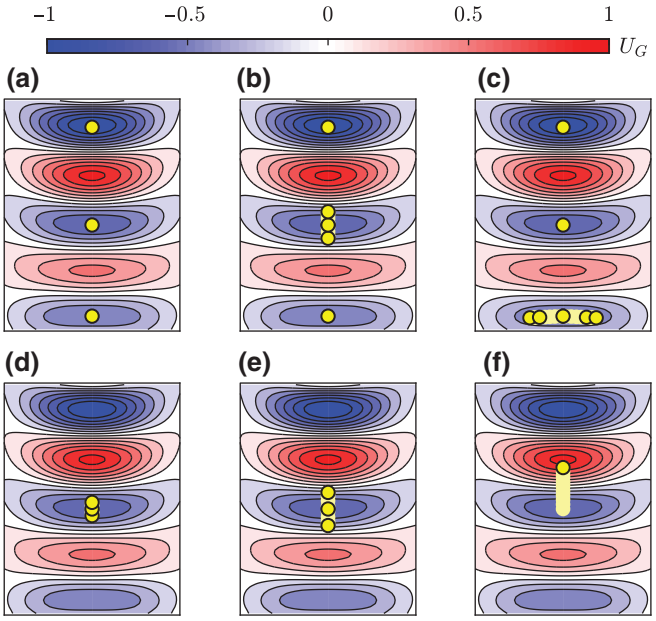

FIG. 1. Illustration of suggested NPM technique. Particles in different locations shown upon a section view of the normalized axisymmetric Gorkov's potential. (a) Particles steadily levitated in the acoustic traps—PE off. (b),(c) Ability to select a specific particle and oscillate it in a desired direction—PE on. (d)–(f) Ability to control the oscillation amplitude; in (f), amplitude is large enough for the particle to escape the trap upwards – PE on.

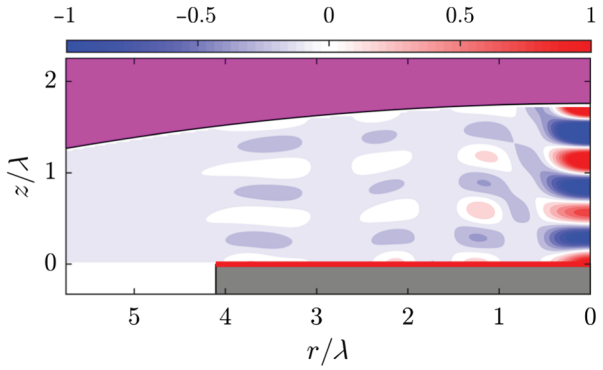

FIG. 2. Section view of a single-axis axisymmetric acoustic levitator and normalized Gor'kov's potential numerically computed using OpenBEM [31]. Three ellipsoid-shaped acoustic "traps" (blue) on the symmetry axis. Ultrasonic emitter (red) located at the bottom and curved reflecting surface shown at the top (magenta).

Nowadays, single-axis standing wave acoustic levitators are commonly used for holding particles and droplets in place [6]. They are usually realized by an acoustic emitter and a concave reflector [2,18,27] or two opposing emitters [28,29], although researchers have shown that they can be realized by an array of transducers [7,20,30]. Here, the former type of levitator, discussed in Sec. III D 1 is analyzed. The objective of this work is to develop a NPM technique based on parametric excitation (PE [30–32]) and to demonstrate it experimentally. PE can oscillate particles resting in acoustic traps without contact, external intervention, or oscillation of the trap position [20]. The levitated particles are parametrically excited by modulating the effective stiffness. Stiffness modulation is realized by a multifrequency excitation of the emitter's amplitude surface velocity, v, as detailed in Sec. III D 2. The suggested approach differs from previous studies because particle oscillations are generated without translation or rotation of the traps and can operate with a single transducer; hence, reducing the required hardware. In addition, the acoustic trap's positions are predetermined, which further reduces the method's complexity.

In the following, the dynamics of a rigid spherical particle in an axisymmetric ellipsoid-shaped trap is investigated. This kind of trap is usually generated along the symmetry axis of single-axis levitators, as shown in Fig. 2. Moreover, only the dynamics along the symmetry (gravity) axis is studied, while the particle is parametrically excited. To do so, a nonlinear lumped-parameters model, which captures the nonlinear forces, is first derived in Sec. III A. Then, its dimensionless governing parameters are estimated from measured data. To generate several traps along the symmetry axis, numerical simulations are used to design the acoustic cavity, where the standing wave field is generated, as described in Sec. III D 1. These simulations are used as a qualitative means to design the reflector geometry and are not used to estimate the resultant stiffness, as in Ref. [20]. The latter is obtained experimentally because PE requires precise excitation frequencies, beyond what can be obtained by a numerical model. Numerical models provide a qualitative confirmation of the physical phenomena, but are incapable of accurately describing the inevitable imperfections of the emitter and boundary conditions.

Once the model parameters are estimated, an asymptotic analytical solution is derived using the method of multiple scales [32–34], and compared with experimentally and numerically obtained solutions, which show good agreement. Lastly, we demonstrate the ability to parametrically excite acoustically levitated particles. We experimentally show that, by employing principal parametric resonance (PPR) [32,34] on the levitated particle, it can oscillate with a large enough amplitude to allow it to escape the trap. Furthermore, PPR is a very narrow banded phenomenon [35], and almost no two acoustic traps are identical (Figs. 1–3); therefore, when multiple particles are being levitated in different traps, it is possible to oscillate a specific selected particle, as we demonstrate in Sec. IV C. The suggested approach may lead to the ability to control multiple particles in 3D by a single or a small number of transducers.

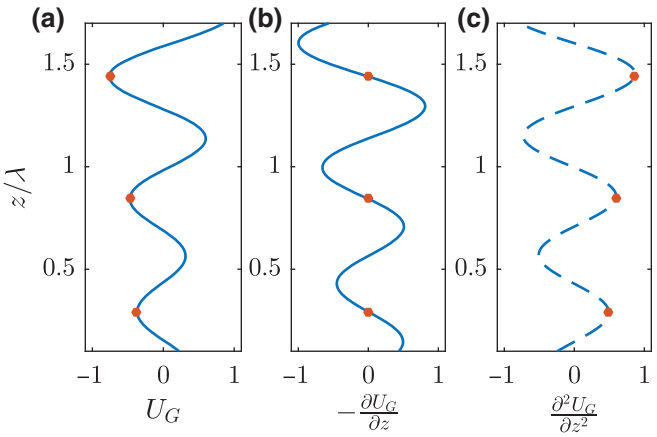

FIG. 3. Numerically computed Gor'kov's potential and its derivatives along the symmetry axis for the geometry shown in Fig. 2; circular markers highlight equilibrium positions (acoustic traps) in the absence of gravity. (a) Normalized Gor'kov's potential, (b) normalized ARF in the z direction, and (c) normalized linear stiffness in the z direction, $k_z = \partial^2 U_G/\partial z^2$.

II. DESCRIPTION OF THE NPM TECHNIQUE

Figure 1 shows a section view (enlargement of Fig. 2) of an axisymmetric normalized Gor'kov's potential [36] and the particles' position in different scenarios. Figure 1(a) depicts three particles levitating steadily in three distinct traps, when no PE is employed. It is clearly visible that each trap is distinct and that the stiffness in the vertical (Fig. 3) and horizontal directions is different. Therefore, at each trap, identical particles have two distinct natural frequencies and associated mode shapes, six in total. The specific in-plane vibration mode is unknown due to symmetry and for simplicity is referred to as horizontal.

The suggested NPM technique utilizes PE to oscillate a selected particle in a certain direction, according to the distinct natural frequency. By modulating the stiffness at a frequency close to double that of the natural frequency, the particle resonates at the natural frequency—PPR. Figures 1(a) and 1(b) illustrate the ability to choose a particle and resonate it in a certain direction in space. Notably, in Fig. 1(c), due to the large amplitude and gravity, the particle motion is not purely horizontal. Furthermore, by controlling the PE frequency and magnitude, the oscillation amplitude is controllable. Figures 1(d) and 1(e) illustrate oscillations of a single particle in the vertical direction with different amplitudes. By further increasing the oscillation amplitude, the particle can escape the trap in the oscillations direction, as shown in Fig. 1(f).

To generate PPR, it is sufficient to know the natural frequencies and associated damping ratios, as the governing equation reduces to the damped Mathieu equation [32]. However, to control the oscillation amplitude, a model that takes into consideration the nonlinearities must be derived; otherwise, the analytical solution produces a diverging motion and a closed-form solution of the steady-state response cannot be obtained.

III. GOVERNING EQUATIONS AND METHODS

A. Deriving the governing equation of motion

The levitated particles considered in this work are rigid spheres with a radius much smaller than that of the acoustic wavelength $r_s \ll \lambda$; therefore, the ARFs can be approximated by Gor'kov's theory [36]. According to this theory, the ARFs are computed as $\mathbf{F} = -\nabla U_G$, where U_G is regarded as the potential energy due to the ultrasonic wave field and approximated as

$$U_G = 2\pi r_s^3 \left[\frac{1}{3\rho_0 c_0^2} \left(1 - \frac{\rho_0 c_0^2}{\rho_s c_s^2} \right) \langle p_1^2 \rangle - \rho_0 \left(\frac{\rho_s - \rho_0}{2\rho_s + \rho_0} \right) \langle \mathbf{u}_1 \cdot \mathbf{u}_1 \rangle \right]. \quad (1)$$

Here, $\rho_{0/s}$ are the medium and sphere densities, respectively; $c_{0/s}$ are the sound speeds in the medium and sphere, respectively; p_1 is the linear pressure; $\mathbf{u}_1$ is the particle velocity; and $\langle \bullet \rangle$ is the time average of $\bullet$. Once the linear pressure is computed, $\mathbf{u}_1$ can be computed from the linear continuity equation, $\mathbf{u}_1 = -\int \nabla p_1/\rho_0 dt$. Furthermore, p_1 is proportional to the transducer's surface velocity amplitude, v; therefore, $U_G \propto v^2$. Because ARFs are estimated by time averaging a fast phenomenon that occurs at ultrasonic frequencies, particle manipulation methods are at least one timescale slower. The governing equations in the presence of gravity, g, without dissipation are derived by employing Hamilton's principal. Considering the spherical particle movement in an acoustic trap along the levitator symmetry axis (i.e., z, $r = 0$) and adding the nonlinear damping force, F_d, *ad hoc*, the governing equation is

$$m\ddot{z} - F_d(\dot{z}) + \frac{\partial U_G}{\partial z} = -mg, \quad (2)$$

where m is the sphere's mass and $\dot{\bullet} \triangleq \partial \bullet / \partial t$. Expanding the nonlinear forces as a power series around the equilibrium position, z_{eq} (i.e., acoustic trap), up to the third power, in accordance with previous works [20,24,26], and defining dimensionless parameters, Eq. (2) simplifies to (see the derivation stages, along with the definitions of u, ε, γ, $\zeta_\bullet$, $\kappa_\bullet$, Ω, and F in Appendix A)

$$u'' + 2\varepsilon\zeta_1 u' + \varepsilon\zeta_2 u'^2 + \varepsilon^2\zeta_3 u'^3 + [1 + \varepsilon\gamma\cos(\Omega\tau)] \times (u + \varepsilon\kappa_2 u^2 + \varepsilon^2\kappa_3 u^3) = \varepsilon\gamma F\cos(\Omega\tau). \quad (3)$$

Here, the dissipative (damping) term coefficients are $\zeta_\bullet$; the linear stiffness is scaled to unity; the nonlinear stiffness terms are $\kappa_\bullet$; and the dimensionless time is $\tau = \omega_n t$, where ω_n is the sphere's natural frequency when small

motions are considered and $\bullet' \equiv \partial/\partial\tau$. In general, the stiffness parameters can be estimated from Gor'kov's theory [6,20] and damping terms, according to Pérez *et al.* [26] or Xie and Vanneste [22]; however, here they are estimated from measurements to obtain better accuracy in the presence of inevitable imperfections.

B. Deriving the required surface velocity amplitude

The nondimensional excitation at frequency $\Omega = \omega_p/\omega_n$ is introduced to the system by modulating the emitter's surface velocity amplitude, $v(t)$, with a multifrequency signal. In general, the emitter may not necessarily vibrate in a pistonlike mode, but in a general frequency-dependent shape, $\Phi(r,\omega)$, dictated by the emitter's surface mode of vibration. It is not required to know $\Phi(r,\omega)$ in order to apply the method, although it is required in the levitator design stage, as discussed in Sec. III D 1. Normally, $\Phi(r,\omega)$ can be precomputed via finite element analysis and, once it is found, the emitter surface velocity can be expressed as $v(t)\Phi(r,\omega)$.

From Eq. (3), it is noticeable that modulating $v(t)$ leads to direct forcing with amplitude γF and PE with magnitude γ. To produce the excitation in Eq. (3), v is modulated as

$$v = v_0\sqrt{1+\alpha\cos(\omega_p t)}\cos(\omega t), \qquad \omega_p \ll \omega \approx 28.56\,\text{kHz}. \tag{4}$$

where $\alpha = \varepsilon\gamma, \omega$ is the Langevin horn transducer's resonance frequency, $\omega_p = \Omega\omega_n$ is the PE frequency, and v_0 is the mean amplitude that allows acoustic levitation [e.g., Fig. 1(a)].

C. Approximate analytical solution

The asymptotic solution is approximated using the method of multiple scales [32–34]. A second-order uniform solution in the following form is sought

$$u(\varepsilon,\tau) = \sum_{n=0}^{2}\varepsilon^n u_n(\tau_0,\tau_1,\tau_2), \quad \tau_n = \varepsilon^n\tau. \tag{5}$$

The fast timescale τ_0 is associated with changes occurring at a frequency close to ω_n, which is scaled to unity. The other slow timescales are associated with amplitude and phase modulations due to damping, resonances, and nonlinearities. Here, we seek the steady-state solution in the presence of PPR (i.e., $\Omega \approx 2$); therefore, the following detuning parameter is defined $\sigma = (\Omega - 2)/\varepsilon$, where $\varepsilon = 10^{-3}$, as detailed in Appendix A. The solution comprises of many frequencies due to the nonlinearities and PE; however, the closest spectral component to the natural frequency dominates and the approximate solution is

$$u = a_0\cos[(\Omega\tau - \psi_0)/2] + O(\varepsilon), \tag{6}$$

where a_0 and ψ_0 depend on the nonlinear parameters, detuning parameter σ, and PE magnitude γ; details of the multiple scales stages that yield Eq. (6) can be found in the Supplemental Material [23].

D. Experimental setup

1. Experimental system

The single-axis ultrasonic levitator experimental rig is shown in Fig. 4, and Fig. 5 depicts four particles levitated along the symmetry axis. It comprises an ultrasonic emitter, which is the plate attached to a shape-optimized Langevin horn [37], serving as a mechanical amplifier, developed locally; a concave 3D-printed reflector; and a laser vibrometer (Polytec OFV-5000 controller with OFV-551 fiber vibrometer), which measures the emitter's velocity. The horn consists of a piezoelectric actuator (Fuji Ceramics FBL28452HS) with a center frequency of 28.5 kHz, resulting in a wavelength of $\lambda = 12.17$ mm in air. Moving and tilting the reflector, which is mounted on a tilt and *XYZ* stage, allows adjustment of the acoustic cavity. In the cavity, expanded polystyrene spheres with a radius of 1–2.5 mm are levitated and oscillated.

The emitter does not oscillate in a pistonlike mode in the operating frequency, but in a Bessel functionlike axisymmetric vibration mode [37]. The horn is a mechanical amplifier designed to operate at its first longitudinal vibration mode and it amplifies the piezoelectric-stack

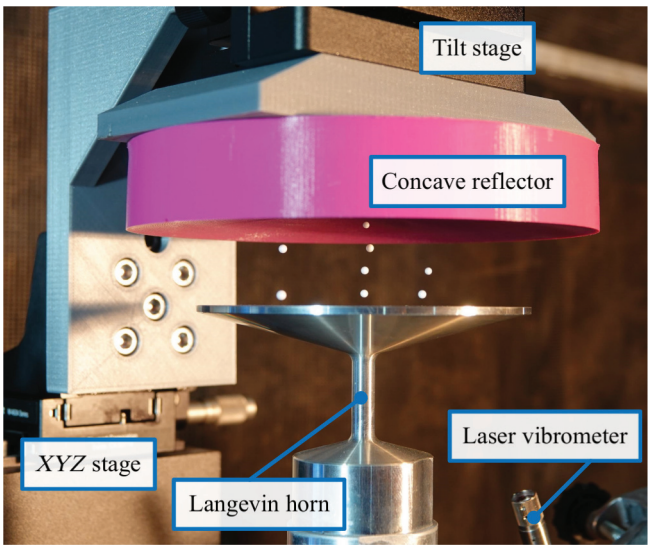

FIG. 4. Single-axis acoustic levitator experimental rig, comprising a Langevin horn, two stages for precise position of the 3D-printed concave reflector, and a vibrometer. The horn and reflector external diameters are 100 and 140 mm, respectively.

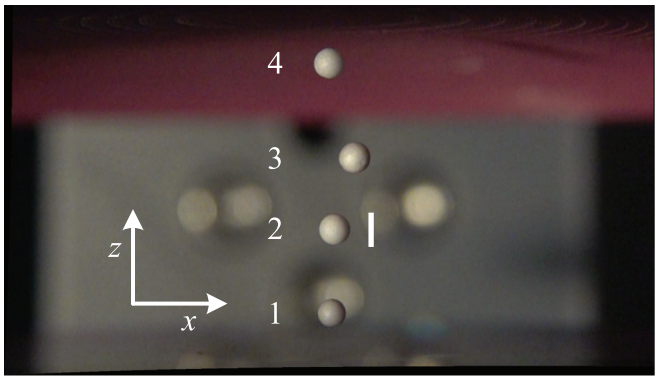

FIG. 5. Acoustic cavity where four expanded polystyrene spheres are levitated; three traps are along the symmetry axis and one is slightly off. Scale bar, 3 mm.

motion; thus, creating large amplitude vibrations at the top surface (i.e., the emitter). The horn and emitter are designed to match the natural frequency and impedance of the piezoelectric actuator. To operate in a pistonlike mode at ultrasonic frequencies, the emitter should be thicker, leading to large inertia, which hinders the efficiency.

In the experimental rig design stage, finite element method (FEM) analysis is used to design the horn and emitter geometry, leading to efficient generation of large amplitude vibrations. Using FEM, the emitter vibration mode shape, $\Phi(r,\omega)$, at resonance is computed and used in a boundary elements (BEM) [38] simulation. In the BEM simulation, the spatial velocity distribution of the emitter, which is highlighted by a red line in Fig. 2, is introduced as the excitation, while the rest of the boundaries are assumed to be rigid. To reduce the computational complexity and take advantage of the problem's symmetry, an axisymmetric BEM simulation is computed with OpenBEM [31]. From the numerically computed linear pressure field, the Gorkov's potential is computed (Figs. 1 and 2). The potential and its derivatives along the symmetry axis are shown in Fig. 3.

The BEM simulation is used as a qualitative tool to design the 3D-printed reflector (e.g., diameter, curvature radius, and depth) and set its distance from the emitter, see Ref. [18]. With the designed reflector, we are able to generate three acoustic traps along the symmetry axis, as shown in Figs. 1 and 2. However, there are slight discrepancies between the simulation and experimental results shown in Figs. 4 and 5; it seems that there are four traps along the symmetry axis. A closer examination reveals that the third trap (Fig. 5) is slightly off axis and the discrepancies may be due to manufacturing imperfections, reflector misalignment, and reflections from the reflector holder shown in Fig. 4. Nevertheless, the discrepancies do not affect the accuracy of the utilized parameters, which are estimated from measured data.

2. Transducer's velocity modulation algorithm

A schematic description of the experimental system depicting the algorithm and signal processing is graphically illustrated in Fig. 6. We employ a fast digital signal processor (DS5203 FPGA Board) with a high-voltage amplifier (A.A. Lab systems LTD A-303) to drive the Langevin horn. We set the modulation parameters α, ω_n, v_0, and Ω according to Eq. (4) and the system's estimated parameters (Table I), which lead to the desired velocity

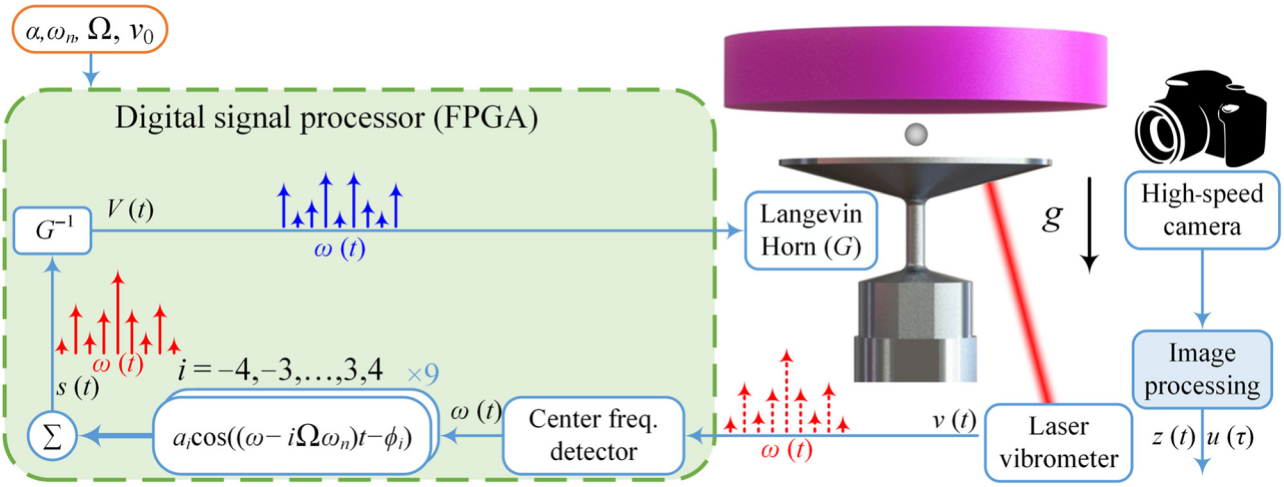

FIG. 6. Schematic description of the experimental system. A laser vibrometer measures the emitter's velocity; modulation and PLL are realized in real time with a fast digital signal processor [field-programmable gate array (FPGA)]. PLL is a type of resonance tracking system used to ensure the base excitation frequency matches the ever-drifting horn's natural frequency. PLL is realized digitally in the FPGA. High-speed camera measures the levitated particle's position; the instantaneous position is estimated using a subpixel resolution algorithm.

TABLE I. Estimated parameter values.

Parameter	Weighted mean	Weighted variance
ω_n	38.69 Hz	0.14
ζ_1	21.920	0.081
ζ_2	−0.14	0.13
ζ_3	0.52	0.34
κ_2	0.144	0.067
κ_3	−19.8	7.3

spectrum of the Langevin transducer. However, modulating the velocity of the horn's surface to achieve PE is not straightforward because (i) the horn is a frequency-dependent dynamic system; thus modulating the input voltage, $V(t)$, will produce velocity modulation, $v(t)$, with a different spectral content, and (ii) the horn's natural frequency is ever drifting, making its response to modulation unpredictable [23,39–41].

To achieve the desired velocity modulation, a dynamic model of the horn is first experimentally generated, G. Next, the first nine harmonics' amplitudes and phases of the desired modulated signal are generated; the center harmonic is the resonance frequency of the horn, $\omega(t)$. Each of these harmonics composing $s(t)$ are then inverted by the experimentally obtained horn's dynamic model (G^{-1}, see Appendix B), to obtain the actual voltage signal, $V(t)$, to be sent to the amplifier. In this way, the dynamics of the horn cancels out the inversion of the excitation signal, producing the desired modulation.

The described method assumes that all harmonics are centered around the horn's constant resonance frequency, ω. However, this frequency drifts considerably over time. To compensate for this time variation, a phase-locked loop (PLL) [42] resonance tracking system is incorporated to ensure that the center frequency always produces a dictated amplitude and phase shifts. Therefore, the center excitation frequency will always be the resonance frequency, despite its slow drift. Because the additional eight sideband harmonic's frequencies, relative to the resonance frequency, are constant, these harmonics drift with $\omega(t)$, facilitating a consistent velocity modulation of the slowly time-varying system.

3. Experimental identification of the governing parameters

To verify the suggested model Eq. (3) numerically and to validate it experimentally, first its parameters should be estimated. The governing nondimensional parameters ω_n, $\zeta_\bullet$, and $\kappa_\bullet$ are estimated from measured data. In all experiments where a single particle is considered, it is levitated in the second trap, as shown in Fig. 5. In this experiment, the PE modulation strength, α, and frequency, Ω, are set to produce large oscillation amplitudes (i.e., enough for the nonlinearities to affect the measured response) and, once the system reaches a steady state, modulation is turned off. Then, the response of the unexcited homogeneous system (i.e., $F=\gamma=0$) to initial conditions is recorded by a high-speed camera (type Sony Cyber-shot DSC-RX10 IV at 960 fps), and the sphere's position is extracted by a calibrated image processing and an efficient subpixel image registration algorithm (e.g., Ref. [43]). The parameters are estimated by minimizing the deviation between the measured response and a numerical simulation of the model using a global optimization algorithm [44]. The process is repeated for ten experiments and the results are averaged according to the minimum variance approach, and are given in Table I (further details are provided in Ref. [23]).

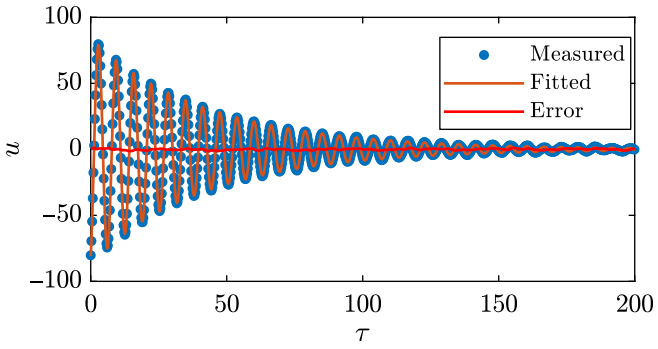

FIG. 7. Response of the homogenous system (levitated particle) to initial conditions. Dimensionless measured displacement, fitted response, and error versus dimensionless time.

It is noticeable that the system is indeed nonlinear, exhibiting a softening behavior because the equivalent nonlinear stiffness is negative [45,46] (i.e., $9\kappa_3 - 2[2\zeta_2^2 + 5\kappa_2(\zeta_2+\kappa_2)] < 0$, see Supplemental Material [23]). Figure 7 shows the measured displacement, fitted curve, and residual dimensionless variables for Video 1 [23]. It is important to note that the parameters are fitted for maximum dimensionless displacement and velocity $u_{\max} \approx u'_{\max} \approx 80$, which is approximately 1 mm and 38 mm s^{-1}. Furthermore, although $\zeta_2 < 0$, the total damping is always dissipative and its actual force always draws energy from the particle motion.

IV. RESULTS AND DISCUSSION

A. Frequency and modulation magnitude sweeps

To validate the derived nonlinear model and demonstrate the ability to control the oscillation amplitude, frequency and modulation magnitude sweeps of the dominant harmonic term close to the natural frequency are measured experimentally. During the frequency sweeps, the system is parametrically excited at $\Omega \approx 2$, and modulated with $\alpha = 0.12$, leading to PPR-driven oscillations. The dominant harmonic term amplitude, a_0, is at half the excitation frequency [see Eq. (6)], as shown in Fig. 8(a), where the

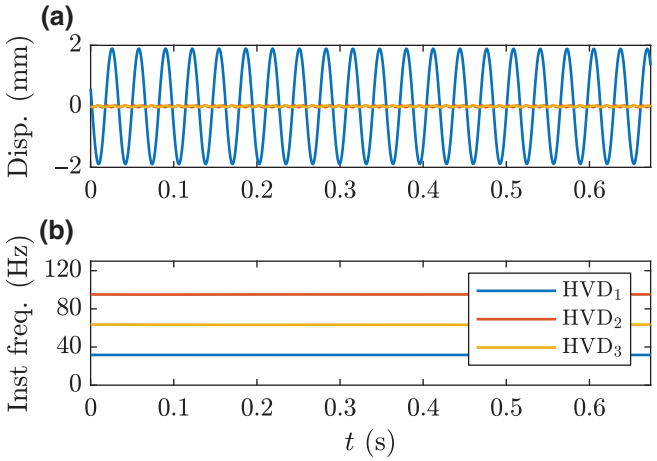

FIG. 8. Steady-state response to PPR when $\omega_p = 63.36$ Hz. (a) Three leading measured displacement components and (b) estimated instantaneous frequencies using the HVD method.

Hilbert vibration decomposition (HVD) [47] is utilized. By extracting the first three dominant components, as shown in Fig. 8(b), the corresponding instantaneous frequencies are computed. It is clear from the nontrivial results shown in Fig. 8 that, once the response reaches steady-state, there is one dominant and two considerably smaller harmonic components. The leading term is at half the modulation frequency and is close to the natural frequency, which is predicted to be about 31.68 Hz. The second term is at a modulation frequency of about 63.36 Hz and is related to the direct excitation and quadratic stiffness, κ_2; the third term is at approximately three times the natural frequency of about 95.04 Hz and is attributed to the cubic stiffness, κ_3. These results assist in validating the model that predicts these harmonic terms. Figure 8 shows the data related to Video 2 [23].

The frequency sweep of Fig. 9 shows the results of 24 different experiments, the analytically obtained solution, and numerical simulations. The analytical solution predicts two solution branches, where one is stable and the other is unstable, and cannot be captured experimentally. Moreover, the analytical solution predicts that the amplitude continues to grow when the detuning parameter, σ, is decreased, while the simulated and experimental solutions decay to the trivial stable solution. It is important to note that the parameters are estimated only up to $u_{\max} \approx u'_{\max} \approx 80$, which is depicted by the red dashed line; therefore, agreement is expected only for $0 \leq u \leq 80$. However, the results are in a good agreement up to higher amplitudes and, in general, the model captures the softening behavior and rate of amplitude growth versus frequency detuning.

During the modulation magnitude sweep, the system is subjected to PPR ($\Omega \approx 2$) and modulated with increasing values of α. When the system reaches steady-state, the dominant harmonic amplitude term, a_0, is estimated and it is depicted versus $\alpha/\alpha_{\text{th}}$ in Fig. 10, where $\alpha_{\text{th}} = 4\varepsilon\zeta_1$ is the theoretical threshold that allows PPR [23]. Figure 10 shows the results of 21 different experiments, analytically obtained solutions, and numerical simulations. As before, two solution branches are predicted analytically, where one is stable and the other is unstable. All solutions predict the initiation of PPR approximately at a theoretical value of $\alpha/\alpha_{\text{th}} = 1$ and the amplitude's growth with increasing values of α. The agreement between various solutions is good; however, a small difference appears as the amplitude grows, for the same reasons as those mentioned previously. The red dashed line represents the amplitude values up to which the parameters are estimated experimentally.

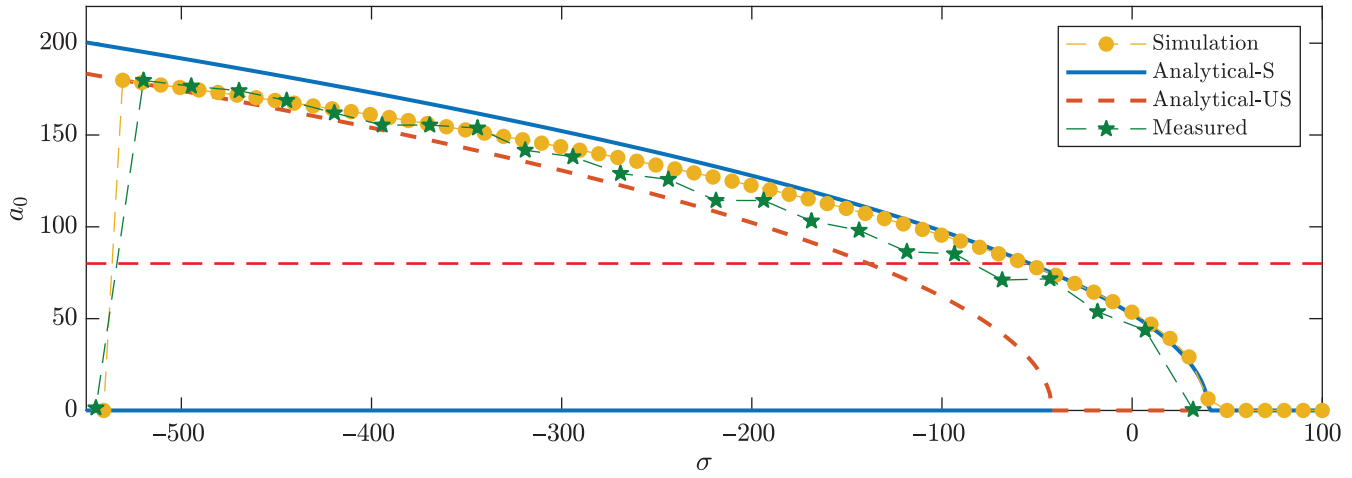

FIG. 9. Frequency sweep. Dimensionless amplitude close to the levitated sphere's natural frequency versus the detuning parameter. Continuous (dashed) lines depict analytically stable (unstable) solution branches, circular markers depict numerically computed amplitudes, and star-shaped markers depict measured amplitudes. The dashed horizontal red line at $a_0 = 80$ depicts the limit up to which the parameters are estimated.

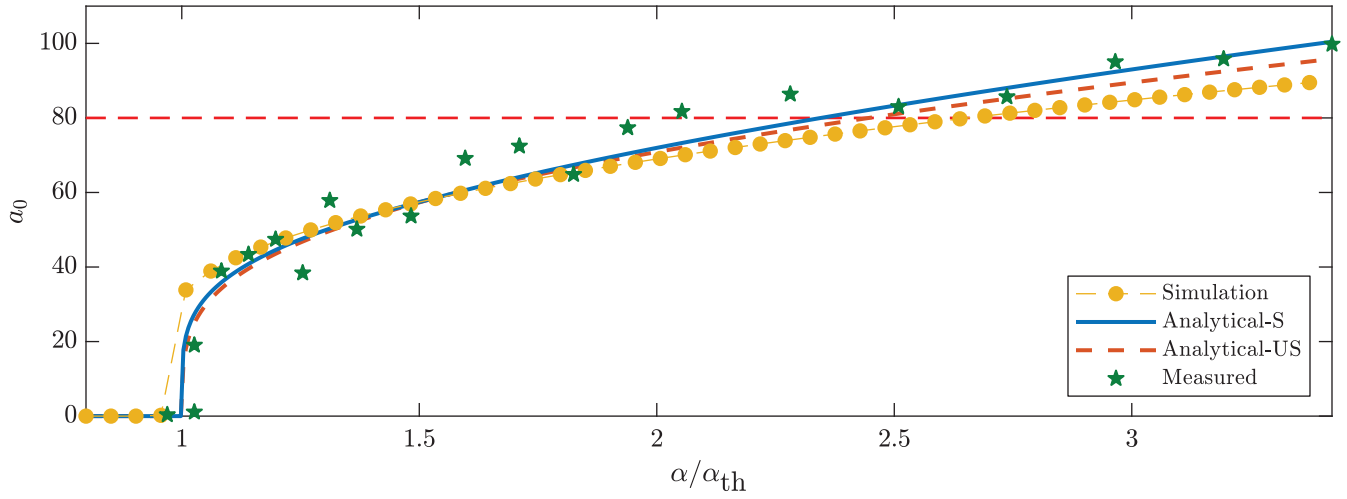

FIG. 10. Modulation magnitude sweep. Dimensionless amplitude close to the levitated sphere's natural frequency versus the normalized modulation amplitude. Continuous (dashed) lines depict analytically stable (unstable) solution branches, circular markers depict numerically computed amplitudes, and star-shaped markers depict measured amplitudes. The dashed horizontal red line at $a_0 = 80$ depicts the limit up to which the parameters are estimated.

B. Escape from a trap

In Sec. IV A, it is shown that oscillation amplitude is controllable. To generate large oscillations, one can gradually reduce the excitation frequency, Ω, or increase the modulation strength, α. Figure 11 shows the instantaneous position of a sphere escaping the trap in the opposite direction to gravity (Video 3 [23]). This is achieved by controlling both the PE frequency and modulation strength.

First, the sphere is parametrically excited with a relatively small α and frequency detuning, σ, is gradually lowered to increase the oscillations' amplitude (Fig. 9). When the sphere is oscillating with large and stable amplitudes, α is considerably increased to enable the jump (Fig. 10). Figure 11 shows that the sphere exits the trap vertically in the z direction, in accordance with the oscillation direction.

C. Excitation of a specific particle

The natural frequency of a homogeneous spherical particle resting in an acoustic trap depends on its mass, $m = 4/3\pi r_s^3 \rho_s$, and the linear stiffness [see Eq. (A2)], which is derived from the trap's geometry [e.g., Fig. 3(c)]. If the mass is changed by a variation in the radius, r_s, and the density, ρ_s, is unchanged, the equilibrium position, z_{eq}, and natural frequency, ω_n, remain the same, as can be deduced from Eqs. (1), (2), and (A2).

However, if the mass is changed by a variation in the density, ρ_s, the equilibrium position and natural frequency do change. Therefore, homogeneous spherical particles made of the same material, with a different radius and resting in the same trap, have the same natural frequency, as long as Gor'kov's theory holds [36].

Multiple traps exist in the acoustic cavity, as numerically predicted (Fig. 2), and Fig. 4 shows some trapped particles. From the numerical results shown in Fig. 3, it is clear that the linear stiffness in the z direction of the three traps along the symmetry axis differ. In the studied configuration, as shown in Fig. 5, three traps along the symmetry axis and another one close to the axis can be approximated as ellipsoids, where each trap is different in terms of stiffness. In addition, there are approximately 12 other toroidal-shaped traps off the symmetry axis that differ from each other. In this section, we focus on the four traps shown in Fig. 5, and take advantage of the PPR's narrow bandwidth to demonstrate the ability to excite specific particles. Four different particles made of expanded polystyrene rest in four different traps, and therefore, have distinct natural frequencies.

To estimate the natural frequency of each particle in the z direction, a frequency sweep is performed during which the stiffness is modulated with a relatively large

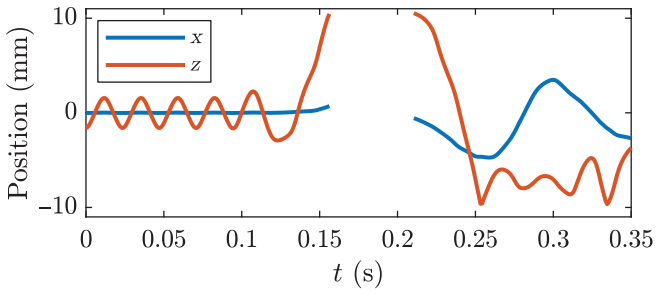

FIG. 11. Instantaneous position of a sphere escaping an acoustic trap (No. 2 in Fig. 5). Blank region is because the sphere is outside the frame.

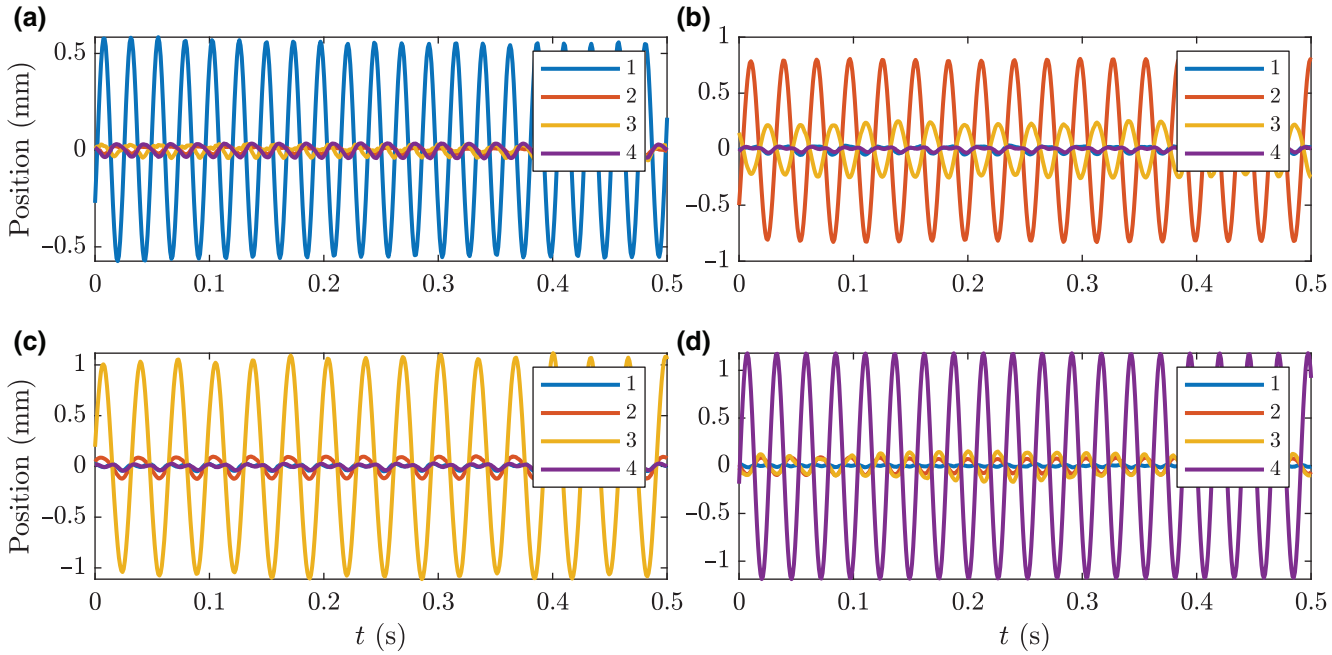

FIG. 12. Experimentally obtained instantaneous position of spheres in the z direction versus time for different PE parameters. PE is tuned to generate PPR of a specific particle, by setting ω_p to approximately twice the relevant natural frequency: (a) 84.5 Hz, (b) 69.5 Hz, (c) 61 Hz, and (d) 77.5 Hz.

amplitude. Video 4 [23] shows the response of the system over a few selected frequencies. It can be seen in Video 4 [23] that there is a frequency band for which the particle in the first trap oscillates laterally; moreover, the lateral oscillations are coupled with the vertical ones, as in Fig. 1(c). This coupling is due to the joint effects of gravity and ellipsoidal trap shape [i.e., as the particle oscillates in plane (r), the stiffness in the z direction changes and the particle sags periodically]. Because the spacing of the frequencies is wider than the PPR's bandwidth (approximately 1.6 Hz, the region of a single stable solution branch where $74.78/\sqrt{2} \leq a_0 \leq 74.78$, Fig. 9), each particle can be excited separately.

The estimated natural frequencies in the z direction of the four particles, as numbered in Fig. 5, are (1) 42.5 Hz, (2) 34.75 Hz, (3) 30.5 Hz, and (4) 38.75 Hz. The ability to excite each particle separately is shown in Fig. 12, which depicts the particles' displacement, when the emitter's velocity is modulated with a different frequency. In Fig. 12(a), the modulation frequency is 84.5 Hz, leading to PPR of the first sphere; in Fig. 12(b), the modulation frequency is 69.5 Hz, leading to PPR of the second sphere; in Fig. 12(c), the modulation frequency is 61 Hz, leading to PPR of the third sphere; and in Fig. 12(d), the modulation frequency is 77.5 Hz, leading to PPR of the fourth sphere. It is noticeable that in each case the parametrically excited sphere has the largest amplitude, while additional spheres have smaller amplitudes due to external forcing and interaction forces [48,49]. Figure 12 depicts the data of Video 5 [23].

V. SUMMARY AND CONCLUSIONS

In this work, we introduce a noncontact particle manipulation technique based on parametric excitation, which takes advantage of the unique spatial shape of the potential and the principle parametric resonance narrow bandwidth to enable one to select a levitated particle and resonate it at a chosen amplitude in a certain direction. To implement the method, an improved analytically lumped parameter model, which takes into consideration nonlinear stiffness and damping terms, is derived.

In recent works, the contribution of acoustic streaming, drag force, and the unique potential geometry giving rise to nonlinear terms are considered and implemented in the models [20,22,24,25]. However, in this work, the linear and nonlinear forces are approximated by expanding the nonlinear forces in a power series that includes all terms up to the third power, which is in accordance with previous works. The parameters of the derived model which are estimated from measured data, facilitates a better understanding of the dynamic behavior because it is analytically solved and it provides the steady-state solution dependency on various parameters. With this model, we are able to implement the NPM technique, accurately control the oscillation amplitude, and predict the softening behavior.

The parameter identification approach adopted here can be implemented for every acoustic levitator; thus, this yields a better understanding of the particle dynamics in the trap. Adopting this approach allows one to avoid the

discrepancies between the ideal theoretical model and real-life experimental system and may enable a refined acoustic levitator design.

PE is generated by periodically modulating the effective stiffness, which is achieved by exciting the emitter's surface velocity amplitude with a time-dependent signal, which is derived from the analytical model. The voltage signal fed to the power amplifier is controlled in real time by a FPGA board, with which the instantaneous horn's resonance frequency is tracked. Moreover, the FPGA is used to generate a unique excitation signal, which compensates for the horn and power amplifier dynamic response; thus, this facilitates the desired PE.

The proposed NPM technique can also be used to generate a fundamental parametric resonance [50], by setting $\Omega \approx 1$, with a sufficiently large α. This is realized during the frequency sweep shown in Video 4 [23]. However, to achieve the same amplitude levels as those in the case of PPR, much stronger modulation of α is needed. This is in agreement with theory, as one can infer from the damped stability charts [51], where PPR is the first instability tongue and the fundamental parametric resonance is the second.

The introduced technique differs from common NPM realizations because the acoustic traps remain fixed in space. Moreover, the ability to control multiple particles by a single actuator is experimentally demonstrated. A possible application of the method will utilize a 3D array of acoustic traps, along with position feedback. The proposed method may be used in the future to control the position of particles discretely, by directional hopping between traps.

ACKNOWLEDGMENTS

A.D. would like to acknowledge generous financial support from the Israeli Ministry of Science and Technology (3-13336) for an Applied Science Scholarship for Engineering Ph.D. Students 2016.

APPENDIX A

Expanding the nonlinear forces in Eq. (2) as a power series to the third order around the equilibrium position, z_{eq}, yields

$$\begin{aligned} &u'' + \frac{c_1}{m\omega_n}u' + \frac{c_2}{m}\lambda\varepsilon u'^2 + \frac{c_3}{m}\lambda^2\varepsilon^2\omega_n u'^3 \\ &\quad + [1 + \alpha\cos(\Omega\tau)] \\ &\quad \times \left(u + \frac{k_2}{k_1}\lambda\varepsilon u^2 + \frac{k_3}{k_1}\lambda^2\varepsilon^2 u^3\right) \\ &= -\frac{v_0^2\alpha k_0}{m\omega_n^2\lambda\varepsilon}\cos(\Omega\tau), \end{aligned} \tag{A1}$$

where

$$\begin{aligned} &F_d(\Delta\dot{z})|_{\dot{z}_{\mathrm{eq}}=0} \approx c_1\Delta\dot{z} + c_2\Delta\dot{z}^2 + c_3\Delta\dot{z}^3 + O(\Delta\dot{z}^3), \\ &\left.\frac{\partial U_G}{\partial z}\right|_{z_{\mathrm{eq}}} \approx v^2[k_0 + k_1\Delta z + k_2\Delta z^2 + k_3\Delta z^3 + O(\Delta z^3)], \\ &\Delta z = z - z_{\mathrm{eq}} = \varepsilon\lambda u, \quad v = v_0\sqrt{1 + \alpha\cos(\Omega\tau)}, \\ &\tau = \omega_n t, \quad \omega_n = v_0\sqrt{\frac{k_1}{m}}, \quad \frac{\partial\bullet}{\partial\tau} = \bullet'. \end{aligned} \tag{A2}$$

where, ε is a small positive scaling parameter (here, $\varepsilon = 10^{-3}$), λ is the acoustic wavelength, $\Omega = \omega_p/\omega_n$ is the scaled parametric excitation frequency by the natural frequency, and $\alpha < 1$ is the modulation strength. The scaled parameters in Eq. (3) are

$$\begin{aligned} &\zeta_1 = \frac{c_1}{2\varepsilon m\omega_n}, \quad \zeta_2 = \frac{c_2\lambda}{m} \quad \zeta_3 = \frac{c_3\lambda^2\omega_n}{m}, \quad \gamma = \frac{\alpha}{\varepsilon}, \\ &\kappa_2 = \frac{k_2}{k_1}\lambda, \quad \kappa_3 = \frac{k_3}{k_1}\lambda^2, \quad F = -\frac{v_0^2\alpha k_0}{m\omega_n^2\lambda\varepsilon}. \end{aligned} \tag{A3}$$

APPENDIX B

The desired velocity spectrum is given by Eq. (4) and to realize it digitally the Fourier series of the slow amplitude modulation is computed as a series expansion for small modulation values, α.

$$\sqrt{1 + \alpha\cos(\omega_p t)} = a_0 + \sum_{n=1}^{4} a_n\cos(n\omega_p t) + b_n\sin(n\omega_p t) \tag{B1}$$

where $b_n \equiv 0$ and a_n are

$$\begin{aligned} &a_0 = 1 - \frac{\alpha^2(64+15\alpha^2)}{1024}, \quad a_1 = \frac{\alpha(32+3\alpha^2)}{64}, \\ &a_2 = -\frac{\alpha^2(16+5\alpha^2)}{256}, \quad a_3 = \frac{\alpha^3}{64}, \quad a_4 = -\frac{5\alpha^4}{1024}. \end{aligned} \tag{B2}$$

Considering the following nine harmonics $\omega_k = \omega + k\omega_p$, $k = -4, -3, \ldots, 3, 4$, the input voltage signal is:

$$\begin{aligned} \frac{V}{v_0} &= \frac{a_4}{2A_1}\cos(\omega_{-4}t - \phi_1) + \frac{a_3}{2A_2}\cos(\omega_{-3}t - \phi_2) \\ &+ \frac{a_2}{2A_3}\cos(\omega_{-2}t - \phi_3) + \frac{a_1}{2A_4}\cos(\omega_{-1}t - \phi_4) \\ &+ \frac{a_0}{A_5}\cos(\omega_0 t - \phi_5) + \frac{a_1}{2A_6}\cos(\omega_1 t - \phi_6) \\ &+ \frac{a_2}{2A_7}\cos(\omega_2 t - \phi_7) + \frac{a_3}{2A_8}\cos(\omega_3 t - \phi_8) \\ &+ \frac{a_4}{2A_9}\cos(\omega_4 t - \phi_9), \end{aligned} \tag{B3}$$

where $A_\bullet$ and $\phi_\bullet$ are the amplitude ratios and phase delays, respectively, computed from the estimated horn's mobility function, G.

[1] E. H. Brandt, Levitation in physics, Sience **243**, 349 (1989).
[2] E. H. Brandt, Suspended by sound, Nature **413**, 474 (2001).
[3] A. Watanabe, K. Hasegawa, and Y. Abe, Contactless fluid manipulation in air: Droplet coalescence and active mixing by acoustic levitation, Sci. Rep. **8**, 10221 (2018).
[4] R. Tuckermann, B. Neidhart, E. G. Lierke, and S. Bauerecker, Trapping of heavy gases in stationary ultrasonic fields, Chem. Phys. Lett. **363**, 349 (2002).
[5] W. J. Xie, C. D. Cao, Y. J. Lü, Z. Y. Hong, and B. Wei, Acoustic method for levitation of small living animals, Appl. Phys. Lett. **89**, 214102 (2006).
[6] M. A. B. Andrade, N. Pérez, and J. C. Adamowski, Review of progress in acoustic levitation, Brazilian J. Phys. **48**, 190 (2018).
[7] L. Cox, A. Croxford, B. W. Drinkwater, and A. Marzo, Acoustic Lock: Position and orientation trapping of non-spherical sub-wavelength particles in mid-air using a single-axis acoustic levitator, Appl. Phys. Lett. **113**, 054101 (2018).
[8] M. Prisbrey and B. Raeymaekers, Ultrasound Noncontact Particle Manipulation of Three-Dimensional Dynamic User-Specified Patterns of Particles in Air, Phys. Rev. Appl. **10**, 034066 (2018).
[9] A. Marzo and B. W. Drinkwater, Holographic acoustic tweezers, Proc. Natl. Acad. Sci. U.S.A. **116**, 84 (2019).
[10] A. Birdsall, U. K. Krieger, and F. N. Keutsch, in *AGU Fall Meet. Abstr.* (2107).
[11] E. A. Crawford, C. Esen, and D. A. Volmer, Real time monitoring of containerless microreactions in acoustically levitated droplets via ambient ionization mass spectrometry, Anal. Chem. **88**, 8396 (2016).
[12] C. A. Rey, D. R. Merkley, G. R. Hammarlund, and T. J. Danley, Acoustic levitation at high temperatures in the microgravity of space, J. Acoust. Soc. Am. **82**, S106 (2005).
[13] E. H. Trinh and K. Ohsaka, Measurement of density, sound velocity, surface tension, and viscosity of freely suspended supercooled liquids, Int. J. Thermophys. **16**, 545 (1995).
[14] R. R. Whymark, Acoustic field positioning for containerless processing, Ultrasonics **13**, 251 (1975).
[15] H. Bruus, Acoustofluidics 7: The acoustic radiation force on small particles, Lab Chip **12**, 1014 (2012).
[16] R. T. Beyer, Radiation pressure—the history of a mislabeled tensor, J. Acoust. Soc. Am. **63**, 1025 (1978).
[17] H. M. Hertz, Standing-wave acoustic trap for nonintrusive positioning of microparticles, J. Appl. Phys. **78**, 4845 (1995).
[18] W. J. Xie and B. Wei, Dependence of acoustic levitation capabilities on geometric parameters, Phys. Rev. E **66**, 026605 (2002).
[19] D. Foresti and D. Poulikakos, Acoustophoretic Contactless Elevation, Orbital Transport and Spinning of Matter in Air, Phys. Rev. Lett. **112**, 024301 (2014).
[20] T. Fushimi, T. L. Hill, A. Marzo, and B. W. Drinkwater, Nonlinear trapping stiffness of mid-air single-axis acoustic levitators, Appl. Phys. Lett. **113**, 034102 (2018).
[21] H. Wijaya, K. Latifi, and Q. Zhou, Two-dimensional manipulation in mid-air using a single transducer acoustic levitator, Micromachines **10**, 257 (2019).
[22] J.-H. Xie and J. Vanneste, Dynamics of a spherical particle in an acoustic field: A multiscale approach, Phys. Fluids **26**, 102001 (2014).
[23] See Supplemental Material at http://link.aps.org/supplemental/10.1103/PhysRevApplied.12.034031 for (1) I. Derivation of the governing EOM, II. Approximate analytical solution, III. Generating the approximated modulation signal, IV. The Langevin horn natural frequency drift, V. Numerical procedure for parameter estimation. (2) Five slow motion videos: Video 1, response to initial conditions; Video 2, steady-state response to principal parametric resonance; Video 3, particle escape from an acoustic trap; Video 4, frequency sweep response of four acoustically levitated particles; and Video 5, oscillation of specific particles.
[24] M. A. B. Andrade, T. S. Ramos, F. T. A. Okina, and J. C. Adamowski, Nonlinear characterization of a single-axis acoustic levitator, Rev. Sci. Instrum. **85**, 045125 (2014).
[25] K. Jia, D. Mei, J. Meng, and K. Yang, Dynamic properties of micro-particles in ultrasonic transportation using phase-controllable standing waves, J. Appl. Phys. **116**, 164901 (2014).
[26] N. Pérez, M. A. B. Andrade, R. Canetti, and J. C. Adamowski, Experimental determination of the dynamics of an acoustically levitated sphere, J. Appl. Phys. **116**, 184903 (2014).
[27] M. A. B. Andrade, F. Buiochi, and J. C. Adamowski, Finite element analysis and optimization of a single-axis acoustic levitator, IEEE Trans. Ultrason. Ferroelectr. Freq. Control **57**, 469 (2010).
[28] J. K. R. Weber, C. A. Rey, J. Neuefeind, and C. J. Benmore, Acoustic levitator for structure measurements on low temperature liquid droplets, Rev. Sci. Instrum. **80**, 83904 (2009).
[29] C. J. Benmore and J. K. R. Weber, Amorphization of Molecular Liquids of Pharmaceutical Drugs by Acoustic Levitation, Phys. Rev. X **1**, 011004 (2011).
[30] A. Marzo, A. Barnes, and B. W. Drinkwater, TinyLev: A multi-emitter single-axis acoustic levitator, Rev. Sci. Instrum. **88**, 085105 (2017).
[31] V. Cutanda Henriquez and P. M. Juhl, in Internoise 2010 (Lisbon, 2010), p. 5796.
[32] A. H. Nayfeh and D. T. Mook, *Nonlinear Oscillations* (John Wiley & Sons, Weinheim, 2008).
[33] A. H. Nayfeh, *Introduction to Perturbation Techniques* (John Wiley & Sons, Weinheim, Germany, 2011).
[34] A. H. Nayfeh, *Perturbation Methods* (John Wiley & Sons, Weinheim, Germany, 2008).
[35] A. Dolev and I. Bucher, Experimental and numerical validation of digital, electromechanical, parametrically excited amplifiers, J. Vib. Acoust. **138**, 061001 (2016).
[36] L. P. Gor'kov, Forces acting on a small particle in an acoustic field within an ideal fluid, Dokl. Akad. Nauk SSSR **140**, 88 (1961).
[37] D. Ilssar, I. Bucher, and N. Cohen, in ISMA 2014 - Int. Conf. Noise Vib. Eng. (Leuven, 2014).
[38] Y. Liu, *Fast Multipole Boundary Element Method: Theory and Applications in Engineering* (Cambridge University Press, New York, NY, USA, 2009).

[39] S. Davis, R. Gabai, and I. Bucher, Realization of an automatic, contactless, acoustic levitation motor via degenerate mode excitation and autoresonance, Sens. Actuators, A **276**, 34 (2018).
[40] M. A. B. Andrade, S. Polychronopoulos, G. Memoli, and A. Marzo, Experimental investigation of the particle oscillation instability in a single-axis acoustic levitator, AIP Adv. **9**, 035020 (2019).
[41] D. Ilssar, I. Bucher, and H. Flashner, Modeling and closed loop control of near-field acoustically levitated objects, Mech. Syst. Signal Process. **85**, 367 (2017).
[42] N. Cermak, S. Olcum, S. C. Wasserman, and S. R. Manalis, US20180245972A1 (27 October 2015).
[43] M. Guizar-Sicairos, S. T. Thurman, and J. R. Fienup, Efficient subpixel image registration algorithms, Opt. Lett. **33**, 156 (2008).
[44] Z. Ugray, L. Lasdon, J. Plummer, F. Glover, J. Kelly, and R. Martí, Scatter search and local NLP solvers: A multistart framework for global optimization, INFORMS J. Comput. **19**, 328 (2007).
[45] A. Dolev and I. Bucher, Optimizing the dynamical behavior of a dual-frequency parametric amplifier with quadratic and cubic nonlinearities, Nonlinear Dyn. **92**, 1955 (2018).
[46] L. D. Zavodney, A. H. Nayfeh, and N. E. Sanchez, The response of a single-degree-of-freedom system with quadratic and cubic non-linearities to a principal parametric resonance, J. Sound Vib. **129**, 417 (1989).
[47] M. Feldman, *Hilbert Transform Applications in Mechanical Vibration* (Wiley, Chichester, West Sussex, United Kingdom, 2011).
[48] G. T. Silva and H. Bruus, Acoustic interaction forces between small particles in an ideal fluid, Phys. Rev. E **90**, 063007 (2014).
[49] A. Hancock, Doctoral dissertation, University of California, 2001.
[50] L. D. Zavodney and A. H. Nayfeh, The response of a single-degree-of-freedom system with quadratic and cubic non-linearities to a fundamental parametric resonance, J. Sound Vib. **120**, 63 (1988).
[51] I. Kovacic, R. Rand, and S. Mohamed Sah, Mathieu's Equation and its generalizations: Overview of stability charts and their features, Appl. Mech. Rev. **70**, 020802 (2018).